Volume 1 | Number 1 | Jan 2013 | Pages 1–100

Nanoscale

www.rsc.org/nanoscale

ROYAL SOCIETY OF CHEMISTRY

ROYAL SOCIETY OF CHEMISTRY

www.rsc.org/nanoscale

Journal Name

ARTICLE

Ultra-fast electron capture by electrosterically-stabilized gold nanoparticles

Khashayar Ghandi[a]*, Alexander D. Findlater[b], Zahid Mahimwalla[a], Connor S. MacNeil[a], Ernest Awoonor-Williams[a], Federico Zahariev[b], Mark S. Gordon[b]*

Ultra-fast pre-solvated electron capture has been observed for aqueous solutions of room-temperature ionic liquid (RTIL) surface-stabilized gold nanoparticles (AuNPs; ~9 nm). The extraordinarily large inverse temperature dependent rate constants ($k_e \sim 5 \times 10^{14}$ M^{-1}s^{-1}) measured for the capture of electrons in solution suggest electron capture by the AuNP surface that is on the timescale of, and therefore in competition with, electron solvation and electron-cation recombination reactions. The observed electron transfer rates challenge the conventional notion that radiation induced biological damage would be enhanced in the presence of AuNPs. On the contrary, AuNPs stabilized by non-covalently bonded ligands demonstrate the potential to quench radiation-induced electrons, indicating potential applications in fields ranging from radiation therapy to heterogeneous catalysis.

Introduction:

Interfacial (solid/liquid) reduction/oxidation reactions involving nanomaterials are generally described in terms of electron transfer (ET) reactions.[1] ET reactions are fundamental to many biological and chemical processes[2–4], with many applications in medicine, energy and chemical industry. It is therefore necessary to investigate ET involving nanomaterials for a wide range of potential biological and chemical applications.

In this work, green chemistry methods were used to synthesize advanced non-covalent stabilized, by RTILs, gold nanoparticles (AuNP) that have been proven here to be excellent functional materials for the extremely fast capture of electrons in water at low concentrations: AuNPs can quench electrons generated by ionizing radiation before they get solvated.

Nanomaterial ET reactions are important in many developing technologies including sensitization,[5] energy transduction in photovoltaics,[6] and catalytic processes including biphasic hydrogenations.[7,8] Therefore potential applications of our results are immense and given the emerging popularity of metal nanoparticles (MNPs) in a number of fields,[9–11] there is a clear incentive to study the details of MNP electron transfer reactions.

The capacity of MNPs to accept electrons was first suggested in the 1990s, when it was found that small clusters of gold, silver, and copper exhibit considerable electron affinities.[12] The subsequent embedding of MNP clusters into mesoporous titania led to the observation that ET from TiO_2 to AuNPs, significantly affected the photocatalytic efficiency of the Au/TiO_2 nanocomposite.[13–15] Bamwenda *et al.* were the first

group to report photocatalytic H_2 generation by Au/TiO_2 and Pt/TiO_2 nanoparticles in an illuminated aqueous 5 M C_2H_5OH suspension,[15] where AuNPs are believed to play a key role, not only in catalytic conversion, but in photoconductance as well.[16] ET also plays a pivotal role in radiation-induced free-radical damage *in vivo*, where the prospect of controlling ET reactions with AuNPs is enticing.

To realize the full potential of MNPs, a complete knowledge of the intricate mechanisms and conditions under which ET is most efficient is needed. Considering the importance of AuNP ET reactions in the above mentioned applications and given the ubiquitous nature of water and its importance in the chemistry of MNPs,[17–22] it is worthwhile to investigate the electron donor-acceptor dynamics of MNPs in aqueous solutions. Fundamental questions need to be addressed, such as the possibility of ET from irradiated solvent molecules to MNPs before the electron reaches thermal equilibrium and the possibility of electron tunneling through the solvent molecular networks to MNPs.

Pulse radiolysis and photoelectron spectroscopy have been used to address such fundamental questions and advanced the understanding of solvated electrons in bulk liquid water[23–25] and electron affinities of atomic clusters;[24] however, the understanding of electrons, the most fundamental reducing agent in solution, in the presence of nanomaterials is still incomplete. Nevertheless, there have been some pioneering early works by Belloni and Mostafavi[24–26] and the Henglein group[27] on nanomaterial radiolysis that presented a procedure for creating small seed particles of gold, and then using radiolysis to further control the exact growth/deposition of additional gold atoms onto these seeds to produce larger

nanoparticles. These studies also showed the proper mechanism of AuNP formation *via* a combination of radiation induced redox reactions along with dimer formation in intermediate redox states. Radiolysis has later been used extensively to reduce metal salts such as Au(III) to Au(0), to form nanoparticles, composites and other nanomaterials. Some examples include incorporating gold nanoparticles into carbon nanotubes by immersing thiol functionalized nanotubes in solutions of gold salts and then using radiolysis to reduce the gold to form AuNP's on the nanotubes.[28] Another unique example is the use of radiolysis to synthesize Cd quantum dots on silk fibers.[29] Radiolysis techniques can also be used to make bimetallic nanoparticles, such as Au/TiO$_2$ photocatalysts in which the Au is supported by a TiO$_2$ core. The NPs are grown on prepared TiO$_2$ NPs by radiolysis to reduce the gold salts on the surface of the TiO$_2$. The resulting particles have good charge separation and have catalytic applications.[13] Radiolysis has also been used to make other bimetallic particles such as gold Pd NPs[30] as a greener method for synthesis, and to make silver nanoparticles for which it was observed that increasing the radiation dose reduced the particle size.[31] Other composites made by radiolysis include gold polymer composites for catalysis,[32] and CS-ZnS quantum dots on chitosan.[33] Radiation induced solvated electrons have also been used as reducing species to form Cr oxide nanoparticles from dissolved dichromate solutions of Cr(VI),[34] and iron oxyhyroxide nanoparticles[35] with low size distributions.

The solvated electron, along with its non-equilibrium "pre-solvated" precursors ("pre-solvated" electrons refer to high energy electrons shortly after ionization, still in the process of equilibrating with the solvent),[36] are implicated in various chemical and biological processes. Given the increasing interest in nanomaterials as adjuvants in medicinal chemistries,[37] there is an incentive to probe the dynamics of electrons and other reactive species in the local environment of aqueous nanomaterials.[38]

Materials and Methods

Materials: Benzyldimethyltetradecylammonium chloride was purchased from TCI-America, sodium borohydride was purchased from Sigma Aldrich and hydrogen tetrachloroaurate [HAuCl$_4$•3H$_2$O] was purchased from Alfa Aesar. All chemicals were used as received without any further treatment. Deionized water used in all syntheses was obtained from a Millipore Milli-Q, with resistivity of 18.2 Mcm at 25 °C. Samples were prepared for µSR by removing dissolved oxygen from the AuNP suspension by repeated bubbling with argon gas. The degassed solution was transferred into a µSR cell under an inert N$_2$ atmosphere.

Synthesis of Gold Nanoparticles: The gold nanoparticles [AuNPs] synthesis was carried out as follows:

In a 250 mL round bottom flask aqueous HAuCl$_4$ 5 mL, 2.5 mmol was stirred at 40 °C under a reduced atmosphere of Nitrogen (Praxair 99.997%) for 15 minutes. Bac-14 (4 g, 10 mmol) was then added to 60 mL water and combined with the

aqueous HAuCl$_4$ solution to produce a yellow-solution. NaBH$_4$ (800 mg, 21 mmol) was added to 15 mL of distilled deionized water and the resulting solution added dropwise to the reaction mixture over several minutes. Reduction was instantaneous and the mixture was allowed to stir under mild heat for 2-3 hours.

Muon Spectroscopy (µSR): Samples were prepared for muon spectroscopy [µSR] by removing dissolved oxygen from the AuNP suspension by repeated bubbling with argon gas. The degassed solution was transferred into a µSR cell under an inert Ar atmosphere and irradiated by high-energy positive muons generated in the M20 muon channel at the TRIUMF lab in Vancouver, British Columbia.

The muon beam arises from pion [π$^+$] decay at rest and possesses ~100% spin-polarization. Thermalization begins as the muon interacts with the AuNP solution and eventually reaches thermal equilibrium towards the end of the radiation track.[10]

The spin of the µ$^+$ is initially polarized opposite to the direction of its momentum [anti-parallel]. Before a muon interacts with the sample, it passes through a counter that sends an electronic signal to a time-digital-converter [TDC] and a counter is incremented, starting a "clock". Interaction with the solution subsequently thermalizes the positive muon. Radiolytic products formed during this process are summarized in the ESI (reactions S5 to S10). The positive muon eventually decays to a positron and neutrino–antineutrino pair. The positron is emitted asymmetrically with respect to the muon spin direction at the time of decay. When the decay positron is detected in a counter, the "clock" is stopped and the time intervals are collected in a histogram. The spectra at TRIUMF were acquired by the use of a transverse magnetic field with respect to the muon spin.

Computational Methods: Electron affinity for bare Au13 clusters was calculated using 2nd order Møller-Plesset perturbation theory (MP2), utilizing the aug-cc-pVTZ basis-set using the GAMESS quantum chemistry software suite.[39,40] Water solvent effects on the AuNP electronic structure were modeled with the Polarizable Continuum Model, PCM.[41–43]

Results and Discussion:

This work is focused on ET reactions between the electron and AuNPs stabilized by benzyldimethyltetradecylammonium chloride (bac-14 [diameter 9 ± 3 nm]), with a surface plasmon resonance (SPR) maximum of λmax ≈ 520 nm (Figures 1, 2). A recent report has shown that bac-14 stabilizes the Au surface through-space by anion and cation interactions (Figure 1).[44] In the present work, to determine the rate of electron capture by AuNP/bac-14 in solution as a function of temperature, positive anti-muons (µ$^+$)[45] were used as spin probes as well as the ionizing radiation. This can be done at low concentrations of AuNP. At very high concentrations (e.g. in a slurry made by adding small amount of water to AuNP solid) it is possible that muons would cause radiation damage to the AuNPs during radiolysis process.[46]

Aqueous suspensions of Au/bac-14 NPs were found to scavenge electrons at unprecedented rates, $k_e = 5 \times 10^{14}$ $M^{-1}s^{-1}$ at μM concentrations. The rate constant reported here is considerably larger than rate constants of reactions involving equilibrated solvated electrons in water, suggesting ET to AuNPs occurs at a rate that competes with the solvation of the ionized electron ("dry electron"/non-equilibrium electrons before solvation). The use of ionic liquids (IL) in the synthesis and suspension of NPs has been reported,[47] however, the use of bac-14 to stabilize AuNPs has only been reported very recently.[44] Non-covalent interactions of ionic liquids and colloidal metals have been known to facilitate catalytic transformations.[11,48] To date, there is little reported on the subject of ET in AuNP/IL systems.[44] The temperature dependence of the electron/AuNP reaction reported here demonstrates the potential of AuNP/IL suspensions to interact with and capture electrons on timescales within solvated electron equilibration times (dry/pre-solvated electron capture).
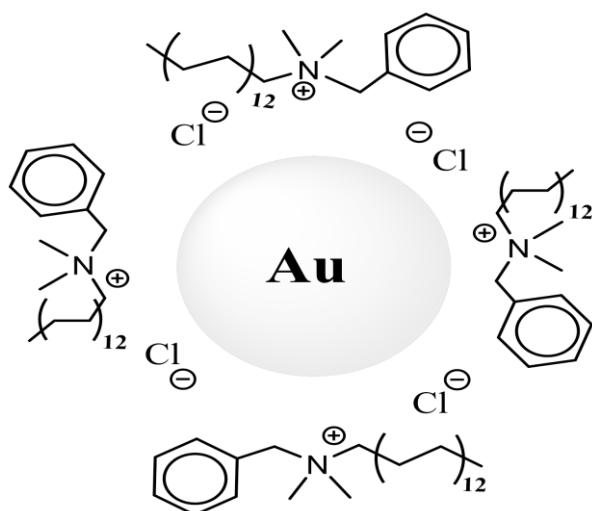

Figure 1. Functionalized AuNPs. Gold atoms are electrosterically stabilized by charged surfactants in water, as opposed to covalent interactions by thiols or thiolate ligands
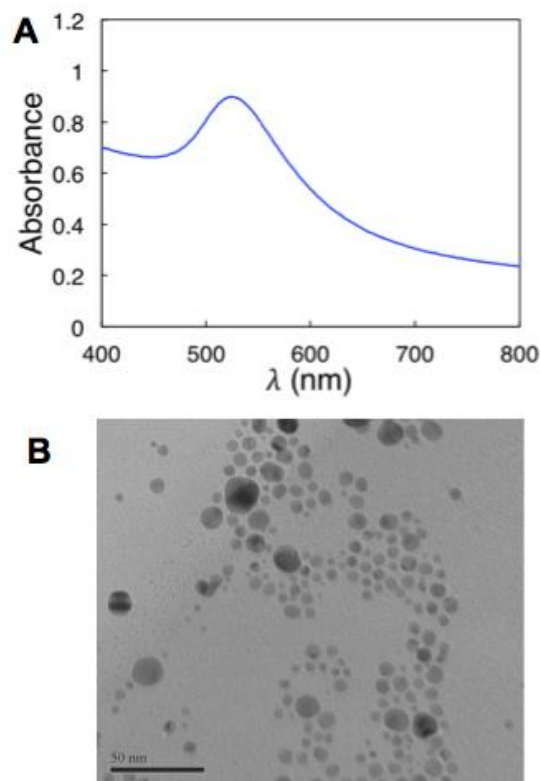

Figure 2. [A] UV-Vis visible spectrum of Au/bac-14 in water with SPR at 520 nm, characteristic of the particle size [44], [B] A representative TEM image of Au/bac-14 in water (see SI): average diameter 9 ± 3 nm.

To deconstruct the complex electron-transfer reactions in water, muon spin rotation (μSR) spectroscopy was employed. Using high-energy anti-muons (μ^+) to generate electrons in solution (*via* ionization), μSR is capable of probing transient radical species through interactions with thermalizing or thermalized anti-muons, serving as spin-probes to study the dynamics of transients.

Previous studies of solvated electrons have involved transient spectroscopic techniques, time-resolved to study the dynamics of these charge carriers and their precursors.[49–51] Work by Percival *et al.*, has shown that the nature and yield of thermalization products are intimately affected by the applied magnetic field, revealing the importance of the solvated electron in the radiation track of anti-muons.[45] A more recent study of water-solvated electrons in the radiation track of positive muons, by means of laser-pulse muon spectroscopy, confirmed the important role that solvated electrons play in the thermalization process.[52]

For the present work, a degassed 0.1 M aqueous solution of dissolved surfactant (bac-14) was used as a reference. In the absence of the AuNPs, the charged surfactant in the reference solution was unable to effectively trap electrons. These electrons therefore combine with positive anti-muons or MuH_2O^+ ions to form transient paramagnetic muonium, an ultra-light hydrogen atom analog [0.11H] that attaches to the

aromatic ring of the surfactant (ESI reactions S5, S7 and S11). Free radicals were characterized through a hyperfine interaction, or coupling between spin-active nuclei and the unpaired electron. The isotropic hyperfine coupling constant [hfcc], is a measure of the unpaired electron density at the nucleus $|\psi[0]|^2$. For muoniated organic radicals, muon hfccs are in the range from a few MHz to several hundred MHz.

The identities of radicals were facilitated using computational chemistry, specifically through comparison of experimental and calculated isotropic Fermi contact coupling of different nuclei. (see ESI supplementary text and table S1).

The addition products (radicals) were determined to be ortho (~ 425 MHz) and ipso (~350 MHz) additions to the bac-14 aromatic ring (Figure 3 and S7), identified by matching theoretical hyperfine-coupling constants of potential products to experimental data [see ESI].
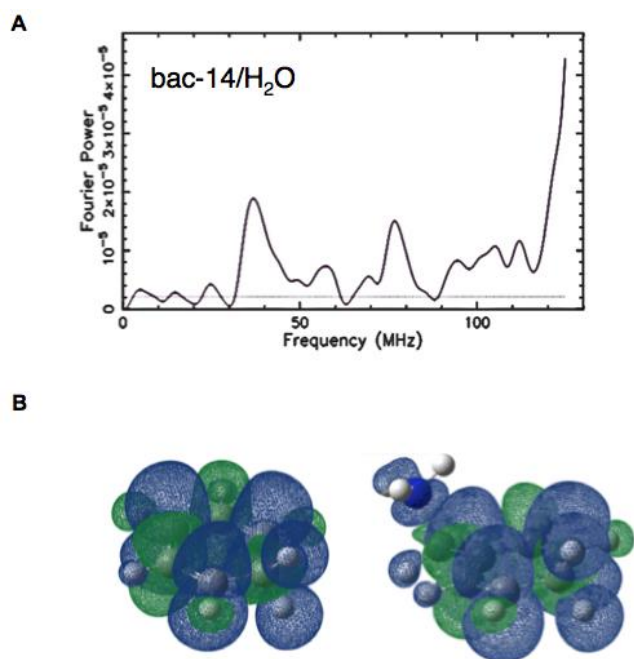

Figure 3. [A] Transverse Field μSR spectrum of bac-14 in water at 274 K, showing two free radicals with muon hfcc of 428 MHz and 349 MHz. The diamagnetic peak is much larger than the two free radical peaks. [B] The calculated spin density of the cyclohexadienyl radical [left] and bac-14 radical [right]. Molecular geometries were optimized at the B3LYP/6-31G* level of theory. The hfcc of the cyclohexadienyl radical is ~515 MHz [53], while the calculated muon hfcc of the para bac-14 radical at 0 K is 441.024 MHz. The calculated hfcc of the *meta* bac-14 radical at 0 K is 455 MHz. For the *ipso* bac-14 radical at 0 K it is 409 MHz.

Measurements for the aqueous AuNP/bac-14 solutions show that the electrons in solution are directly affected by the addition of the AuNPs. The diamagnetic fraction shown in the transverse field spectra (Figure 4) is enhanced for the AuNP solution as compared with the equimolar surfactant control solution under identical experimental conditions (sample geometry and magnetic field).

In aqueous solutions, competition between reactions (ESI S5-S9) in the radiation track determines the anti-muon diamagnetic fraction.[45,54] The observed increase of the diamagnetic fraction for the AuNP solution compared with the reference surfactant

solution suggests considerable electron capture by the AuNPs (ESI S10). Computational results for electron affinities of AuNPs in solution are consistent with the notion that the MuH_2O^+ ion is less effective at capturing pre-solvated electrons than Au/bac-14 NPs. Therefore, we associate the observed increase in diamagnetic fraction to a favorable interaction between the pre-solvated, non-equilibrated electron and AuNPs at small concentrations.
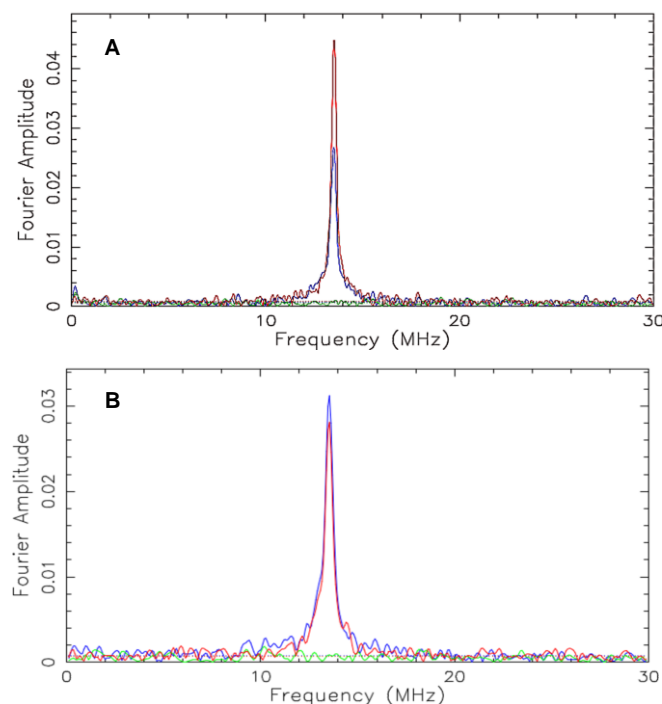

Figure 4. TF spectra (Fourier amplitudes), showing a diminished diamagnetic fraction for the aqueous solution of bac-14. The disparity in the diamagnetic fraction is due to the presence of paramagnetic species, as outlined in Reactions 1, 3, and 4 in ESI. These are either muoniated radicals or Mu. Superior peaks represent aqueous solutions of the cationic surfactant at 298 K and an applied field *H*, 1000 G [A] and 330 K at the same field [B]. Inferior peaks represent aqueous solutions of AuNPs at equivalent temperatures and fields.

The thermalization rate, ν, is the inverse of the time that it takes for high-energy anti-muons to reach thermal equilibrium with the surrounding environment. Since the reaction of solvated and pre-solvated electrons with AuNPs is in competition with this process (see ESI reactions S5-S10), the anti-muon thermalization rate provides the lower-limit to the reaction rate of AuNPs and ionized-electrons in solution (Eq. 1):

$$\nu = k_e \, [AuNP] \qquad\qquad (Eq. 1)$$

where [AuNP] is the AuNP concentration calculated to be 2×10^{-6} M (see ESI) and the muon thermalization rate[45,54] is at least 1 ns^{-1}.

The lower limit of the electron capture rate constant (k_e) for the AuNPs, using Eq. 1, was determined to be 5×10^{14} $M^{-1}s^{-1}$. This large electron capture rate constant suggests the AuNPs are capable of reacting rapidly with the pre-solvated electrons (e_{pre-}), which relax (equilibrate) on ~100 femtosecond

timescales.[36,55] The large electron capture rate constant allows for the exciting prospect of controlling sub-picosecond reactions of reactive intermediates with metal NPs.

The electron capture rate was largest at 298 K and diminished with increasing temperature (see Figure 4 for experimental temperature studies where the diamagnetic amplitudes are different). At temperatures greater than 340 K the diamagnetic amplitudes did not change with the addition of AuNPs. The temperature dependence of the rate constant indicates pre-solvated/non-equilibrium electron capture due to the strong temperature dependence of the electron thermalization/solvation process. At higher temperatures, the increased solvation rate competes[55–60] with AuNP pre-solvated electron capture.

The observed electron capture rates for AuNP/bac-14 are at an order of magnitude larger than those reported for well-known scavengers of pre-solvated electrons, such as KNO_3 (1.2×10^{13} M^{-1} s^{-1}), DMSO (8.1×10^{11} M^{-1} s^{-1}) and isopropanol (2.3×10^{11} M^{-1} s^{-1}), while at significantly lower scavenger concentrations (2×10^{-6} M compared to concentrations as high as 2 M).[61] In addition, 2nd order Møller-Plesset perturbation theory (MP2), utilizing the aug-cc-pVTZ basis-set, predicts the electron capture-reaction free energy (ΔG_{rxn}) and electron affinity (EA) for bare surface Au13 clusters to be seven times that of KNO_3, DMSO and isopropanol in solution (Table 1. All calculations were performed with the GAMESS quantum chemistry software suite.[39,40] Water solvent effects on the AuNP electronic structure were modeled with the Polarizable Continuum Model, PCM).[41–43] The large observed rate constant is also consistent with the size of the AuNPs used in this study compared to the size of molecular species such as KNO_3. This is discussed in detail within the context of a model for diffusion-limited reactions in the SI.

Table 1. Theoretical adiabatic electron affinities (EA in eV) and electron transfer reaction Gibbs free energy differences (ΔG_{rxn} in eV) are presented. All calculations were performed with Moller-Plesset second order perturbation theory [MP2] using the aug-cc-pVTZ and MCP-ATZP basis-sets for non-metal and metal atoms respectively. The Polarizable Continuum Model [PCM] was used to model the aqueous solvent effect. All properties were calculated using GAMESS [39,40].

Electron scavenger	MP2 adiabatic electron affinity EA [eV]	MP2 Gibbs free energy difference ΔG_{rxn} [eV]
$[KNO_3]_{aq}$	0.68	-0.76
$[DMSO]_{aq}$	0.50	-0.53
$[isopropanol]_{aq}$	0.71	-0.78
$[Au_{13}]_{aq}$	5.41	-5.63
$[Au_{13}]_{gas}$	3.85	-
$[Au_{13}]_{gas}$ exp[12]	4.0	-

Among the noble metal clusters of increasing size studied by Smalley,[12] including silver and copper, gold displays the greatest electron affinities as described by ultraviolet photoelectron spectroscopy. In addition, their work suggested a general trend of increase in EA with cluster size, which means even within the activation control limit we should expect much larger rate constants for electron capture by AuNPs compared to KNO_3.

Smalley *et al.* observed that despite the onset of d bands for gold clusters of 1-223 atoms, there is still a noticeable convergence to the bulk EA.[12] For small clusters (<50 atoms), the electronic structure and therefore properties of gold are very sensitive to the number of atoms/electrons. Clusters with odd numbers of atoms exhibit larger electron affinities compared to even-numbered clusters due to the pairing of unpaired electrons and shell filling stabilization effects upon electron capture, with electron affinity trends similar to those of atoms (certain gold clusters are sometimes referred to as "superatoms").[62] For example, calculated MP2 valence natural orbitals for icosahedral Au13 resemble p and d atomic-like orbitals (Figure 5) with occupation numbers that are consistent with Hund's rule. This even-odd oscillation due to spin pairing is damped and eventually washed out with increasing cluster size, however smooth convergence to the bulk is still interrupted by shell closings.[12]
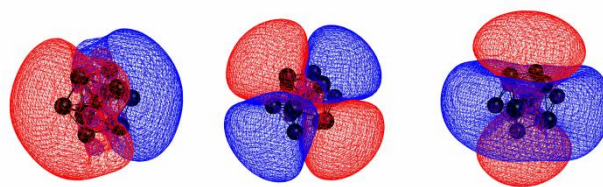

Figure 5. *p*-type (left) and *d*-type (middle and right) MP2 natural orbitals for the icosahedral Au$_{13}$ cluster. A spin-parallel electron occupies each of the five "*d* orbitals" of Au$_{13}$, with addition electrons proceeding to fill the *d*-shell similar to atomic electronic configurations following Hund's rule.

The combination of the presented experimental and computational data, along with the previous works of Smalley's group,[12] suggests AuNPs to be extremely reactive with electrons in water with rates of reaction among the fastest processes in water (faster than charge solvation).

Considering that pre-solvated electrons can contribute significantly to DNA damage,[50,61] AuNPs could have potential therapeutic applications as electron scavengers in radiobiological processes. These results can complement existing applications in which nanoparticles are used as drug delivery and imaging agents for disease detection[63–68] to create multifunctional therapeutic agents. AuNPs can act as general, efficient and fast electron scavengers for various radiation chemistry processes, as the result of large electron scavenging rates (5×10^{14} M^{-1}s^{-1}) that are significantly larger than that of many currently known electron scavengers, at significantly lower concentrations. The compatibility of AuNPs with synthetic inorganic materials as well as biological systems indicates a potential to incorporate Au/bac-14 as an extremely efficient electron acceptor into a variety of environments. Though solid support nanomaterials dominate the ET device and catalysis literature,[69] little is known for aqueous systems and our results suggest future investigations of aqueous AuNP ET and catalytic redox reactions is necessary.

Conclusions

In conclusion, using green chemistry methods advanced non-covalent stabilized gold nanoparticles (AuNP) were synthesized. These nanoparticles are excellent nanoscale functional materials for capturing pre-solvated electrons at low nanoparticle concentrations due to their large radii, high electron affinity towards "naked" AuNPs as compared to dressed AuNPs, and a surfactant that allows the AuNPs to be "naked" when needed, and yet stabilize the nanoparticles in solution (greater than 6 months). In principle, the ability of AuNPs to capture electrons produced by ionizing radiation, allows the possible conversion of ionizing radiation into electricity. Furthermore, these nanoparticles can function as radioprotective materials, preventing solvated and secondary electron based damage induced by ionizing radiation. For example, the nanomaterials can be incorporated into clays and other matrices used to store nuclear waste capturing the secondary electrons that degrade the matrix over time. Their large radii, high electron affinity and surfactant ability to expose the gold core to reactive species also suggest intriguing catalytic behaviour from these nanomaterials.

In biology and medicine, such aqueous nanoparticles can be used to prevent cell damage from secondary electrons generated during radiation therapy. AuNPs (of differing sizes under different conditions) in combination with radiation were shown to prolong survival in tumor-bearing mice however, under low scavenging conditions, radio-protective effects have been observed.[70] Such results encourage further studies on the interactions of radiolytic products and free radicals with AuNPs. Results presented here could not only help unravel the controversies on the role of AuNPs under ionizing radiation, but also challenge the conventional notion that radiation induced damage would be enhanced in the presence of AuNPs. The results presented here also demonstrate the power of muon nanochemistry as a new transdisciplinary frontier for the study of nanomaterial dynamics.

Acknowledgements

Notes and references

^{a} Department of Chemistry & Biochemistry, Mount Allison University, Sackville, NB, Canada, E4L 1G8
Email: kghandi@mta.ca.
^{b} Department of Chemistry and Ames Laboratory, Iowa State University, Ames, Iowa, USA, 50011-3020

1. J. N. Schrauben, R. Hayoun, C. N. Valdez, M. Braten, L. Fridley, and J. M. Mayer, *Science*, 2012, **336**, 1298–301.
2. H. B. Gray and J. R. Winkler, *Annu. Rev. Biochem.*, 1996, **65**, 537–61.
3. J. Evenson and M. Karplus, *Science (80-.).*, 1993, **262**, 1247–1249.
4. J.-M. Saveant, *Pure Appl. Chem.*, 1997, **69**, 269–271.
5. T. Kawawaki, Y. Takahashi, and T. Tatsuma, *Nanoscale*, 2011, **3**, 2865–2867.
6. C. Clavero, *Nat. Photonics*, 2014, **8**, 95–103.
7. J. Dupont, G. S. Fonseca, A. P. Umpierre, P. F. P. Fichtner, and S. R. Teixeira, *J. Am. Chem. Soc.*, 2002, **124**, 4228–4229.
8. G. Vilé and J. Perez-Ramirez, *Nanoscale*, 2014.
9. K. Weintraub, *Nature*, 2013, **495**, 14–16.
10. E. Roduner, *Chem. Soc. Rev.*, 2006, **35**, 583–92.
11. D. Astruc, F. Lu, and J. R. Aranzaes, *Angew. Chem. Int. Ed. Engl.*, 2005, **44**, 7852–72.
12. K. J. Taylor, C. L. Pettiette-Hall, O. Cheshnovsky, and R. E. Smalley, *J. Chem. Phys.*, 1992, **96**, 3319.
13. A. Primo, A. Corma, and H. García, *Phys. Chem. Chem. Phys.*, 2011, **13**, 886–910.
14. M. Cargnello and B. T. Diroll, *Nanoscale*, 2014, **6**, 97–105.
15. G. R. Bamwenda, S. Tsubota, T. Nakamura, and M. Haruta, *J. Photochem. Photobiol. A Chem.*, 1995, **89**, 177–189.
16. H. Nakanishi, K. J. M. Bishop, B. Kowalczyk, A. Nitzan, E. a Weiss, K. V Tretiakov, M. M. Apodaca, R. Klajn, J. F. Stoddart, and B. a Grzybowski, *Nature*, 2009, **460**, 371–5.
17. S. Roy, G. Palui, and A. Banerjee, *Nanoscale*, 2012, 4, 2734.
18. A. M. López Marzo, J. Pons, D. A. Blake, and A. Merkoçi, *Biosens. Bioelectron.*, 2013, **47**, 190–8.
19. S. Jiang, K. Y. Win, S. Liu, C. P. Teng, Y. Zheng, and M.-Y. Han, *Nanoscale*, 2013, **5**, 3127–48.
20. H. C. Chen, B. J. Hwang, F. Der Mai, Y. C. Liu, C. M. Lin, H. S. Kuo, D. S. Chou, M. J. Lee, K. H. Yang, C. C. Yu, J. R. Chen, T. Y. Lo, H. Y. Tsai, C. P. Yang, C. Wang, H. T. Hsieh, and J. Rick, *ACS Nano*, 2014, **8**, 2704–2713.
21. J. C. L. Chow, M. K. K. Leung, and D. A. Jaffray, *Phys. Med. Biol.*, 2012, **57**, 3323–31.

22. H. Razzaq, R. Qureshi, and D. J. Schiffrin, *Electrochem. commun.*, 2014, **39**, 9–11.

23. K. R. Siefermann, Y. Liu, E. Lugovoy, O. Link, M. Faubel, U. Buck, B. Winter, and B. Abel, *Nat. Chem.*, 2010, **2**, 274–9.

24. L. François, M. Mostafavi, J. Belloni, J.-F. Delouis, J. Delaire, and P. Feneyrou, *J. Phys. Chem. B*, 2000, **104**, 6133–6137.

25. L. François, M. Mostafavi, J. Belloni, and J. A. Delaire, *Phys. Chem. Chem. Phys.*, **3**, 4965–4971.

26. E. Gachard, H. Remita, J. Khatouri, B. Keita, L. Nadjo, and and J. Belloni, *New J. Chem.*, 1998, **22**, 1257–1265.

27. A. Henglein and D. Meisel, *Langmuir*, 1998, **14**, 7392–7396.

28. A. M. Showkat, K.-P. Lee, A. I. Gopalan, S.-H. Choi, and Y. C. Nho, *Diam. Relat. Mater.*, 2007, **16**, 1688–1692.

29. S. Chang, B. Kang, Y. Dai, and D. Chen, *Mater. Lett.*, 2008, **62**, 3447–3449.

30. K. Roy and S. Lahiri, *Anal. Chem.*, 2008, **80**, 7504–7.

31. K. Naghavi, E. Saion, K. Rezaee, and W. M. M. Yunus, *Radiat. Phys. Chem.*, 2010, **79**, 1203–1208.

32. C.-H. Zhu, Z.-B. Hai, C.-H. Cui, H.-H. Li, J.-F. Chen, and S.-H. Yu, *Small*, 2012, **8**, 930–6.

33. S.-Q. Chang, B. Kang, Y.-D. Dai, H.-X. Zhang, and D. Chen, *Nanoscale Res. Lett.*, 2011, **6**, 591.

34. L. M. Alrehaily, J. M. Joseph, A. Y. Musa, D. A. Guzonas, and J. C. Wren, *Phys. Chem. Chem. Phys.*, 2013, **15**, 98–107.

35. P. A. Yakabuskie, J. M. Joseph, P. Keech, G. A. Botton, D. Guzonas, and J. C. Wren, *Phys. Chem. Chem. Phys.*, 2011, **13**, 7198–206.

36. M. H. Elkins, H. L. Williams, A. T. Shreve, and D. M. Neumark, *Science*, 2013, **342**, 1496–9.

37. A. J. Mieszawska, W. J. M. Mulder, Z. a Fayad, and D. P. Cormode, *Mol. Pharm.*, 2013, **10**, 831–47.

38. E. Ju, Z. Liu, Y. Du, Y. Tao, J. Ren, and X. Qu, *ACS Nano*, 2014, **8**, 6014–6023.

39. M. W. Schmidt, K. K. Baldridge, J. A. Boatz, S. T. Elbert, M. S. Gordon, J. H. Jensen, S. Koseki, N. Matsunaga, K. A. Nguyen, S. Su, T. L. Windus, M. Dupuis, and J. A. Montgomery, *J. Comput. Chem.*, 1993, **14**, 1347–1363.

40. M. S. Gordon and M. W. Schmidt, in *Theory and Applications of Computational Chemistry: the first forty years*, eds. C. E. Dykstra, G. Frenking, K. S. Kim, and G. E. Scuseria, Elsevier Inc., Amaterdam, 2005, pp. 1167–1189.

41. J. Tomasi, B. Mennucci, and R. Cammi, *Chem. Rev.*, 2005, 105, 2999–3093.

42. D. G. Fedorov, K. Kitaura, H. Li, J. H. Jensen, and M. S. Gordon, *J. Comput. Chem.*, 2006, **27**, 976–985.

43. M. S. Gordon, D. G. Fedorov, S. R. Pruitt, and L. V. Slipchenko, *Chem. Rev.*, 2012, 112, 632–672.

44. M. Farren-Dai, E. Awoonor-Williams, C. S. MacNeil, Z. Mahimwalla, and K. Ghandi, *Chem. Phys. Lett.*, 2014, **610-611**, 331–334.

45. P. W. Percival, *J. Chem. Phys.*, 1980, **72**, 2901.

46. V. G. Storchak, J. H. Brewer, D. G. Eshchenko, P. W. Mengyan, O. E. Parfenov, and D. Sokolov, *J. Phys. Conf. Ser.*, 2014, **551**, 012016.

47. P. Migowski and J. Dupont, *Chemistry*, 2007, **13**, 32–9.

48. J. Huang, T. Jiang, B. Han, H. Gao, Y. Chang, G. Zhao, and W. Wu, *Chem. Commun.*, 2003, 1654.

49. C. Chachaty and E. Hayon, *Nature*, 1963, **200**, 59–60.

50. E. Alizadeh and L. Sanche, *Chem. Rev.*, 2012, **112**, 5578–602.

51. C.-R. Wang, T. Luo, and Q.-B. Lu, *Phys. Chem. Chem. Phys.*, 2008, **10**, 4463–70.

52. K. Ghandi, I. P. Clark, J. S. Lord, and S. P. Cottrell, *Phys. Chem. Chem. Phys.*, 2007, **9**, 353–9.

53. D. Yu, P. W. Percival, J.-C. Brodovitch, S.-K. Leung, R. F. Kiefl, K. Venkateswaran, and S. F. J. Cox, *Chem. Phys.*, 1990, **142**, 229–236.

54. P. Percival, E. Roduner, and H. Fischer, *Chem. Phys.*, 1978, **32**, 353–367.

55. A. Migus, Y. Gauduel, J. Martin, and A. Antonetti, *Phys. Rev. Lett.*, 1987, **58**, 1559–1562.

56. B. C. Garrett, D. A. Dixon, D. M. Camaioni, D. M. Chipman, M. A. Johnson, C. D. Jonah, G. A. Kimmel, J. H. Miller, T. N. Rescigno, P. J. Rossky, S. S. Xantheas, S. D. Colson, A. H. Laufer, D. Ray, P. F. Barbara, D. M. Bartels, K. H. Becker, K. H. Bowen, S. E. Bradforth, I. Carmichael, J. V Coe, L. R. Corrales, J. P. Cowin, M. Dupuis, K. B. Eisenthal, J. A. Franz, M. S. Gutowski, K. D. Jordan, B. D. Kay, J. A. Laverne, S. V Lymar, T. E. Madey, C. W. McCurdy, D. Meisel, S. Mukamel, A. R. Nilsson, T. M. Orlando, N. G. Petrik, S. M. Pimblott, J. R. Rustad, G. K. Schenter, S. J. Singer, A. Tokmakoff, L.-S. Wang, C. Wettig, and T. S. Zwier, *Chem. Rev.*, 2005, **105**, 355–90.

57. J. M. Warman, M. P. De Haas, and J. B. Verberne, *J. Phys. Chem.*, 1980, **84**, 1240–1248.

58. J. M. Warman and C. D. Jonah, *Chem. Phys. Lett.*, 1981, **79**, 43–46.

59. M. P. De Haas, M. Kunst, J. M. Warman, and J. B. Verberne, *J. Phys. Chem.*, 1983, **87**, 4089–4092.

60. J. M. Warman, M. Kunst, and C. D. Jonah, *J. Phys. Chem.*, 1983, **87**, 4292–4294.

61. J. Nguyen, Y. Ma, T. Luo, R. G. Bristow, D. A. Jaffray, and Q.-B. Lu, *Proc. Natl. Acad. Sci. U. S. A.*, 2011, **108**, 11778–83.

62. M. Walter, J. Akola, O. Lopez-Acevedo, P. D. Jadzinsky, G. Calero, C. J. Ackerson, R. L. Whetten, H. Grönbeck, and H. Häkkinen, *Proc. Natl. Acad. Sci. U. S. A.*, 2008, **105**, 9157–9162.

63. L. K. Bogart, G. Pourroy, C. J. Murphy, V. Puntes, T. Pellegrino, D. Rosenblum, D. Peer, and R. Lévy, *ACS Nano*, 2014, **8**, 3107–3122.

64. E. C. Dreaden, A. M. Alkilany, X. Huang, C. J. Murphy, and M. A. El-Sayed, *Chem. Soc. Rev.*, 2012, **41**, 2740–79.

65. S. Parveen, R. Misra, and S. K. Sahoo, *Nanomedicine*, 2012, **8**, 147–66.

66. J. a Webb and R. Bardhan, *Nanoscale*, 2014, 2502–2530.

67. L. Ma, M. Kohli, and A. Smith, *ACS Nano*, 2013, 7, 9518–9525.

68. Y. Huang, S. He, W. Cao, K. Cai, and X.-J. Liang, *Nanoscale*, 2012, 4, 6135.

69. X. Liu, L. He, Y.-M. Liu, and Y. Cao, *Acc. Chem. Res.*, 2014, **47**, 793–804.

70. S. Jain, D. G. Hirst, and J. M. O'Sullivan, *Br. J. Radiol.*, 2012, **85**, 101–13.